Active Load-Modulated Devices: A General PA Network Solution Identifying Highly Efficient Lineariser Architectures

Anton N. Atanasov, *Student Member, IEEE,* Mark S. Oude Alink, *Senior Member, IEEE,* Frank E. van Vliet, *Senior Member, IEEE*

***Abstract*—We present a general analytical solution for the active input impedances of a given N-port impedance network as a function of the loading of its ports by either active or passive devices. To demonstrate the simplicity and ease of use of our approach we derive the input impedance equations of a conventional Balanced Power Amplifier (BPA) and the Load-Modulated Balanced Amplifier (LMBA) and the effects of mismatching the output load. We next focus on the properties of the hybrid coupler and present a general heuristic of categorization and identification of a missing topology. This missing topology is the load-modulated linearizer (LML), which utilizes active load-modulation to absorb individual out-of-band AM/AM intermodulation distortion (IMD) components at the output of a power amplifier. When properly designed, the LML requires only slightly more additional power as the IMD power it absorbs, making it very efficient. It retains the power conservation properties of the LMBA and achieves better linearization than an equivalent DPD system, at a very low power and complexity penalty. As the LML operates at the output of the nonlinear PA, it can independently target individual tones, which gives it a better bandwidth.**

***Index Terms*—LMBA, LML, 5G, active input impedance, active load-modulation, linearization techniques**

I. Introduction

HIGH efficiency in power amplifier (PA) systems [1] comes at the cost of increased distortion, resulting in high in-band (IB) and, often more limiting, out-of-band (OOB) distortion in the form of amplitude to amplitude (AM/AM) and amplitude to phase (AM/PM) distortion. This necessitates a compromise in the form of increased output back-off (OBO) power levels and consequently significantly lower drain efficiency (DE) and power-added efficiency (PAE). Developing ways of mitigating the efficiency penalty due to OBO is an active field of study [2] with the Doherty PA (DPA) [3], Outphasing [4] and the Load-Modulated Balanced Amplifier (LMBA) [5] designs used in telecom being well-known multi-transistor PA examples. This is important for e.g. base stations where increasing output power allows for better range and thus, fewer base stations needed, and the improved efficiency benefits the heat budget management by wasting less power as heat. High efficiency is also critical for battery-constrained devices such as mobile phones as well as for heat-constrained space systems. The most widely used linearization process for telecommunication applications is digital predistortion (DPD). Unfortunately, DPD becomes less and less effective as the transmit PA operates at higher compression levels, as the correction necessary to counteract the non-linear effects can grow without bounds [6]. In contrast, AM/PM correction requires phase rotation, which is still possible with DPD even in compression. Thus, there is a clear need to develop a more systematic analysis of load-modulation mechanisms and further exploration of ways to remove AM/AM distortion from PAs operating at high compression levels.

This work presents two main ideas. First, in section II we present a clear and systematic closed-form solution for the active input impedance and current relations of any N-port microwave structure with an arbitrary number of loaded ports. The derivation shares some conceptual similarities with how the active antenna element input impedance is calculated, however those results are usually interpreted in the S-parameter domain within the antenna array field [7]–[9]. We demonstrate the usefulness of the analysis by re-deriving the LMBA equations in a more straightforward manner. We apply our approach to extend the existing analysis to also account for output load mismatch, such as due to antenna mutual coupling in arrays. Such practical considerations are very useful for current and future developments of multi-transistor PAs in MIMO environments [10]. Finally, we present a conceptual overview of the similarities and constraints between systems which use a quadrature hybrid coupler to highlight a top-level approach of identifying and classifying new device topologies.

And second, in Section III, we present an extended analysis of the load-modulated linearizer (LML) [11], which is a variation of the LMBA concept [5], [12]–[14]. The LML absorbs unwanted IMD products, while keeping the main tones unaffected. It shares similarities with feed-forward systems as the linearization is achieved at the output of the PA instead of the input. In this regard the proposed system is similar to other coupler-based devices such as balanced amplifiers (BPAs) and diode linearisers (DL) used for analog predistortion [15], [16]. We provide a detailed derivation of the mechanisms with which active load-modulation can be used to both couple desired power to the output load and absorb unwanted power, such as OOB AM/AM distortion, at the output of an amplifier. We show the optimal conditions under which the LML can

This paper is an expanded version from the 2022 IEEE BCICTS, Phoenix, AZ USA, 16-19 October 2022.

Anton N. Atanasov, Mark S. Oude Alink, and Frank E. van Vliet are with the Integrated Circuit Design Group, University of Twente, Enschede 7522 NB, Netherlands (e-mail: a.n.atanasov@utwente.nl).

Frank E. van Vliet is also with the Defense, Safety and Security, TNO, The Hague 2597 AK, Netherlands.

Manuscript received November 15, 2022; revised August XX, 2022.

linearize a PA and prove that the necessary control power is significantly lower than the output power of the main PA itself. We present a set of design equations which describe the linearisation mechanism and the overall system efficiency of the LML.

In Section IV we describe the proposed LML system and validate its performance by linearizing a PA, which amplifies two narrowband tones, while operating in strong compression. We are able to achieve more than 30dB suppression of both the IM3 and IM5 tones without interfering with the two main tones. This presents a common scenario for next generation radar and telecom systems, where DPD solutions still struggle. Next, we benchmark the LML against a DPD solution and highlight both advantages and disadvantages of either system. Finally, in Section V we summarise our work and present several concluding remarks.

II. General Solution of the Active Input Impedance

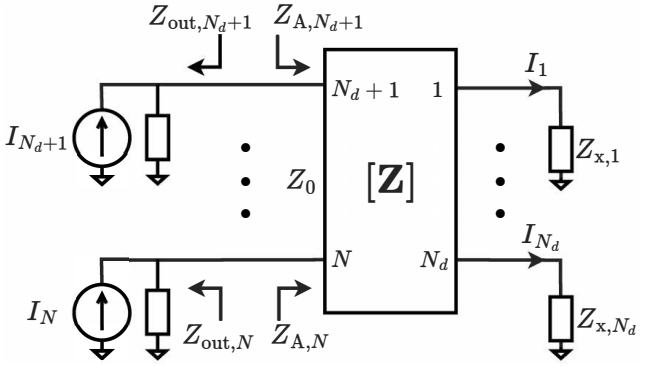

Fig. 1. Topology of a general N-port passive network. Ports 1 through N_d are connected to arbitrary complex loads. Ports $N_d + 1$ through N are connected to current sources with known output impedances, representing matched transistors.

A passive N-port microwave network is shown in Fig. 1. We illustrate a general configuration where some of the ports are connected to arbitrary complex loads, while the rest are connected to current sources with known output impedances, representing transistors. The network has a characteristic impedance of Z_0, and is described by an $N \times N$ impedance (open circuit) matrix, $\mathbf{Z} \in \mathbb{C}^{N \times N}$. The complex loads are defined as $\vec{Z}_{\text{x}} = [Z_{\text{x},1}, \ldots, Z_{\text{x},N_d}]^T$ with $\vec{Z}_{\text{x}} \in \mathbb{C}^{N_d \times 1}$, where the superscript ^{T} denotes the transpose. The currents at each port are defined as $\vec{I} = [I_1, \ldots, I_{N_d}, \ldots, I_N]^T$ with $\vec{I} \in \mathbb{C}^{N \times 1}$ and are assumed to flow into the network. The currents I_1 through I_{N_d} are due to the loads $\vec{Z}_{\text{x}}$ and the currents I_{N_d+1} through I_N are independent sources with a defined amplitude and phase, which serve as an approximation of matched active devices at some bias or compression point. The current sources have known output impedances $\vec{Z}_{\text{out}} = [Z_{\text{out},N_d+1}, \ldots, Z_{\text{out},N}]^T$ with $\vec{Z}_{\text{out}} \in \mathbb{C}^{(N-N_d)\times 1}$, which are matched to the optimal load impedance, Z_{opt}, of the active device using an output matching network (OMN), as shown in Fig. 2.

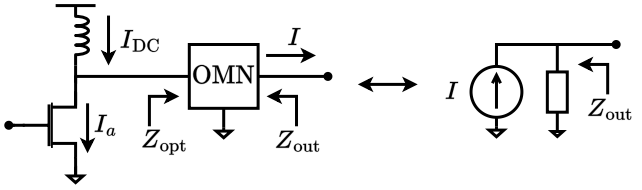

Fig. 2. Arbitrary matched active device, having optimum load impedance Z_{opt} matched to Z^*_{out}, represented as a current source with output impedance Z_{out}.

The relation between $\mathbf{Z}$ and $\vec{I}$ produces the port voltages $\vec{V} = [V_1, \ldots, V_{N_d}, \ldots, V_N]^T$ with $\vec{V} \in \mathbb{C}^{N \times 1}$, which are measured with respect to the common ground connection

$$\mathbf{Z}\vec{I} = \vec{V}. \tag{1}$$

The input impedance of each active port is $\vec{Z}_{\text{A}} = [Z_{\text{A},N_d+1}, \ldots, Z_{\text{A},N}]^T$ with $\vec{Z}_{\text{A}} \in \mathbb{C}^{(N-N_d)\times 1}$. When several active devices are connected to the network they begin to influence each other simultaneously, resulting in $\vec{Z}_{\text{A}}$ being actively load-modulated. This simultaneous interdependence between all active devices is more readily solvable using matrix algebra than with conventional circuit analysis techniques.

A. Active and Passive Current Partitioning

Our goal is to express the input impedance of the active ports, $\vec{Z}_{\text{A}}$, as a function of the active current sources only, such that we fully describe the active load-modulation behaviour. For that purpose we partition the current vector $\vec{I}$ into a passive subvector, $\vec{I}_{\text{P}} = [I_1, \ldots, I_{N_d}]^T$, and an active subvector, $\vec{I}_{\text{A}} = [I_{N_d+1}, \ldots, I_N]^T$. The voltage vector $\vec{V}$ is similarly partitioned into a passive subvector $\vec{V}_{\text{P}} = [V_1, \ldots, V_{N_d}]^T$, and an active subvector $\vec{V}_{\text{A}} = [V_{N_d+1}, \ldots, V_N]^T$, such that

$$\vec{I} = \begin{bmatrix} \vec{I}_{\text{P}} \\ \vec{I}_{\text{A}} \end{bmatrix} \quad \text{and} \quad \vec{V} = \begin{bmatrix} \vec{V}_{\text{P}} \\ \vec{V}_{\text{A}} \end{bmatrix}. \tag{2}$$

The rows and columns of the impedance matrix $\mathbf{Z}$ must be rearranged depending on which ports of the network are active and passive (as will be explicitly shown in Example 1 and Example 2 further in this section), so as to remain consistent with (1) and (2). The impedance matrix $\mathbf{Z}$ is then partitioned into 4 submatrices, whose dimensions depend on the length of N_d and N

$$Z_0 \begin{bmatrix} \mathbf{A} & \mathbf{B} \\ \mathbf{C} & \mathbf{D} \end{bmatrix} \begin{bmatrix} \vec{I}_{\text{P}} \\ \vec{I}_{\text{A}} \end{bmatrix} = \begin{bmatrix} \vec{V}_{\text{P}} \\ \vec{V}_{\text{A}} \end{bmatrix}, \tag{3}$$

where

$$\mathbf{A} = \begin{bmatrix} Z_{1,1} & & Z_{1,N_d} \\ \vdots & \ddots & \vdots \\ Z_{N_d,1} & & Z_{N_d,N_d} \end{bmatrix}$$
$$\mathbf{B} = \begin{bmatrix} Z_{1,N_d+1} & & Z_{1,N} \\ \vdots & \ddots & \vdots \\ Z_{N_d,N_d+1} & & Z_{N_d,N} \end{bmatrix}$$
$$\mathbf{C} = \begin{bmatrix} Z_{N_d+1,1} & & Z_{N_d+1,N_d} \\ \vdots & \ddots & \vdots \\ Z_{N,1} & & Z_{N,N_d} \end{bmatrix} \quad (4)$$
$$\mathbf{D} = \begin{bmatrix} Z_{N_d+1,N_d+1} & & Z_{N_d+1,N} \\ \vdots & \ddots & \vdots \\ Z_{N,N_d+1} & & Z_{N,N} \end{bmatrix}.$$

The subvector $\vec{V}_{\mathrm{P}}$ describes the voltage across $\vec{Z}_{\mathrm{x}}$ due to $\vec{I}_{\mathrm{P}}$

$$\vec{V}_{\mathrm{P}} = \quad \mathrm{diag}\{\vec{Z}_{\mathrm{x}}\}\vec{I}_{\mathrm{P}}, \quad (5)$$

where $\mathrm{diag}\{\vec{Z}_{\mathrm{x}}\}$ is a diagonal loading matrix constructed from $\vec{Z}_{\mathrm{x}}$. The negative sign indicates that the currents $\vec{I}_{\mathrm{P}}$ flow out of the network. As $\vec{V}_{\mathrm{P}}$ is linearly dependent on $\vec{I}_{\mathrm{P}}$, we can incorporate the external passive loads $\vec{Z}_{\mathrm{x}}$ into the network and express their contribution using only $\vec{I}_{\mathrm{P}}$. Substituting (5) into (3) and combining like terms yields the loaded port representation

$$Z_0 \begin{bmatrix} (\mathbf{A}+\mathbf{X}) & \mathbf{B} \\ \mathbf{C} & \mathbf{D} \end{bmatrix} \begin{bmatrix} \vec{I}_{\mathrm{P}} \\ \vec{I}_{\mathrm{A}} \end{bmatrix} = \begin{bmatrix} \vec{0} \\ \vec{V}_{\mathrm{A}} \end{bmatrix}, \quad (6)$$

where

$$\mathbf{X} = \frac{1}{Z_0}\mathrm{diag}\{\vec{Z}_{\mathrm{X}}\} \quad (7)$$

is the normalized loading matrix w.r.t. Z_0. Assuming that the submatrix $(\mathbf{A}+\mathbf{X})$ is invertible, we obtain a closed-form expression of how $\vec{I}_{\mathrm{P}}$ is dependent on $\vec{I}_{\mathrm{A}}$

$$\vec{I}_{\mathrm{P}} = \quad (\mathbf{A}+\mathbf{X})^{-1}\mathbf{B}\vec{I}_{\mathrm{A}}. \quad (8)$$

Substitution of $\vec{I}_{\mathrm{P}}$ into the rest of the system allows to express the active voltages $\vec{V}_{\mathrm{A}}$ across the open ports N_d+1 through N solely in terms of the active currents $\vec{I}_{\mathrm{A}}$

$$\vec{V}_{\mathrm{A}} = Z_0\left(\mathbf{D} \quad \mathbf{C}(\mathbf{A}+\mathbf{X})^{-1}\mathbf{B}\right)\vec{I}_{\mathrm{A}}. \quad (9)$$

This matrix relation is also called the Schur complement of $(\mathbf{A}+\mathbf{X})$ in the loaded port representation of $\mathbf{Z}$ [17]. Finally, the closed-form expression for the input impedance $\vec{Z}_{\mathrm{A}}$ of the active ports is found by normalizing each port voltage with its corresponding port current, giving us

$$\vec{Z}_{\mathrm{A}} = \mathrm{diag}\{\vec{I}_{\mathrm{A}}\}^{-1}\vec{V}_{\mathrm{A}}. \quad (10)$$

The above analysis and its closed-form solutions allow for a systematic investigation and computation of the input impedance of every active port of an arbitrary N-port impedance network. A key aspect of the presented formulation is the ability to directly evaluate the influence load mismatch (e.g. antenna loading due to mutual coupling) has on the $\vec{Z}_{\mathrm{A}}$ in systems with two or more active devices such as BPAs, DPAs and others. The analysis procedure can be summarized as follows:

1) Design microwave network and corresponding Z-matrix;
2) Define active $\vec{I}_{\mathrm{A}}$ and passive $\vec{I}_{\mathrm{P}}$ current vectors;
3) Define loading vector $\vec{Z}_{\mathrm{x}}$;
4) Rearrange $\mathbf{Z}$ based on $\vec{I}_{\mathrm{A}}$ and $\vec{I}_{\mathrm{P}}$;
5) Compute $\vec{I}_{\mathrm{P}}$, $\vec{V}_{\mathrm{A}}$, and $\vec{Z}_{\mathrm{A}}$;
6) Choose expressions for $\vec{I}_{\mathrm{A}}$ which take advantage of active load-modulating properties and give desired $\vec{Z}_{\mathrm{A}}$.

B. Mismatch and Power Relations

The power wave active reflection coefficient seen by an active device looking into its corresponding port n, when both of them are complex-valued, is [18]

$$\Gamma_{\mathrm{A},n} = \frac{Z_{\mathrm{A},n} - Z_{\mathrm{out},n}}{Z_{\mathrm{A},n} + Z_{\mathrm{out},n}}, \quad (11)$$

which can be expressed more generally in vector form as

$$\vec{\mathbf{\Gamma}}_{\mathrm{A}} = \left(\vec{Z}_{\mathrm{A}} - \vec{Z}_{\mathrm{out}}\right) \quad \mathrm{diag}\{\vec{Z}_{\mathrm{A}} + \vec{Z}_{\mathrm{out}}\}^{-1}, \quad (12)$$

where $\circ$ is the Hadamard product (element-wise multiplication) and $\vec{\mathbf{\Gamma}}_{\mathrm{A}} \in \mathbb{C}^{(N-N_d)\times 1}$ whose entries are $\vec{\mathbf{\Gamma}}_{\mathrm{A}} = [\Gamma_{\mathrm{in},N_d+1}, \ldots, \Gamma_{\mathrm{in},N}]$. When the input impedances $\vec{Z}_{\mathrm{A}}$ are the complex conjugate of the devices' output impedances $\vec{Z}_{\mathrm{out}}$ we achieve the conditions for maximum power transfer.

Knowing the input impedance $\vec{Z}_{\mathrm{A}}$ of the active ports allows us to compute the power delivered by the current sources

$$P_{\mathrm{in},n} = \frac{1}{2}|I_{\mathrm{A},n}|^2\,\mathrm{Re}\{Z_{\mathrm{A},n}\}, \quad (13)$$

which can also be expressed in vector form as

$$\vec{P}_{\mathrm{in}} = \frac{1}{2}\mathrm{diag}\{\vec{I}_{\mathrm{A}}\}\mathrm{diag}\{\vec{I}_{\mathrm{A}}\}^{*}\,\mathrm{Re}\{\vec{Z}_{\mathrm{A}}\}. \quad (14)$$

Similarly, knowledge of the current vector $\vec{I}_{\mathrm{P}}$ allows us to compute the amount of power flowing out of every passive port

$$\vec{P}_{\mathrm{out}} = \frac{1}{2}\mathrm{diag}\{\vec{I}_{\mathrm{P}}\}\mathrm{diag}\{\vec{I}_{\mathrm{P}}\}^{*}\,\mathrm{Re}\{\vec{Z}_{\mathrm{x}}\}. \quad (15)$$

Example 1: The Balanced Amplifier

To illustrate the simplicity of our matrix technique in deriving the active input impedances of a network we consider the ubiquitous BPA configuration, whose output part is shown in Fig. 3. It consists of two active devices having quadrature phase shift connected to ports 2 and 4 of an ideal 3dB quadrature hybrid coupler. Port 3 serves as the isolated port and port 1 is the output port. The 4-port Z-matrix of the ideal 3dB quadrature hybrid [5], [19] together with its current and voltage relations is

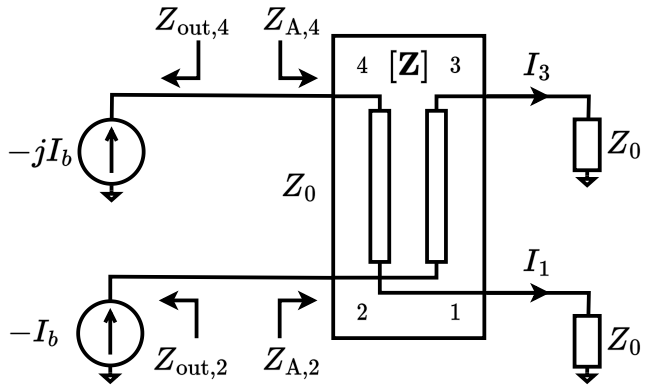

Fig. 3. Conventional BPA configuration. The two active devices are visualized as current sources with finite output impedance Z_{out}. The sources are connected to ports 2 and 4, the output is at port 1 and the isolated port is 3.

$$Z_0 \begin{bmatrix} 0 & 0 & j & j\sqrt{2} \\ 0 & 0 & j\sqrt{2} & j \\ j & j\sqrt{2} & 0 & 0 \\ j\sqrt{2} & j & 0 & 0 \end{bmatrix} \begin{bmatrix} I_1 \\ I_2 \\ I_3 \\ I_4 \end{bmatrix} = \begin{bmatrix} V_1 \\ V_2 \\ V_3 \\ V_4 \end{bmatrix}. \quad (16)$$

We define the passive and active current vectors to be

$$\vec{I}_{\text{P}} = \begin{bmatrix} I_3 \\ I_1 \end{bmatrix} \text{ and } \vec{I}_{\text{A}} = \begin{bmatrix} I_2 \\ I_4 \end{bmatrix} = \begin{bmatrix} I_b \\ jI_b \end{bmatrix}. \quad (17)$$

Ports 1 and 3 are terminated with matched loads

$$\vec{Z}_{\text{x}} = \begin{bmatrix} Z_0 \\ Z_0 \end{bmatrix} \quad (18)$$

and so the normalized loading matrix becomes

$$\mathbf{X} = \frac{1}{Z_0} \begin{bmatrix} Z_0 & 0 \\ 0 & Z_0 \end{bmatrix} = \mathbf{I}. \quad (19)$$

The rows and columns of the impedance matrix $\mathbf{Z}$ are rearranged to reflect $\vec{I}_{\text{P}}$ and $\vec{I}_{\text{A}}$ (see Eq. (4)) giving us

$$\begin{aligned} \mathbf{A} = \mathbf{D} &= \begin{bmatrix} 0 & j \\ j & 0 \end{bmatrix} \\ \mathbf{B} = \mathbf{C} &= \begin{bmatrix} j\sqrt{2} & 0 \\ 0 & j\sqrt{2} \end{bmatrix}. \end{aligned} \quad (20)$$

Computing $\vec{I}_{\text{P}}$ using (8) yields the currents flowing into the output loads

$$\begin{bmatrix} I_3 \\ I_1 \end{bmatrix} = \begin{bmatrix} j\sqrt{2}/2 & \sqrt{2}/2 \\ \sqrt{2}/2 & j\sqrt{2}/2 \end{bmatrix} \begin{bmatrix} I_b \\ jI_b \end{bmatrix} = \begin{bmatrix} 0 \\ \sqrt{2}I_b \end{bmatrix}, \quad (21)$$

which shows that, under perfect conditions, the currents delivered by both active devices are combined and flow into the matched load at port 1, and none into the isolated port 3. Using (9) we evaluate the voltages $\vec{V}_{\text{A}}$ across the active ports

$$\vec{V}_{\text{A}} = Z_0 \begin{bmatrix} 1 & 0 \\ 0 & 1 \end{bmatrix} \begin{bmatrix} I_b \\ jI_b \end{bmatrix}. \quad (22)$$

Finally, the well-known active input impedances $\vec{Z}_{\text{A}}$ of a BPA are obtained using (10)

$$\begin{aligned} Z_{\text{A},2} &= Z_0 \\ Z_{\text{A},4} &= Z_0. \end{aligned} \quad (23)$$

The power delivered to the network by each current source $\vec{I}_{\text{A}}$ is found using (14)

$$\begin{aligned} P_{\text{in},2} &= \frac{1}{2}\text{Re}\{Z_{\text{A},2}\}I_b^2 = \frac{1}{2}Z_0 I_b^2 \\ P_{\text{in},4} &= \frac{1}{2}\text{Re}\{Z_{\text{A},4}\}I_b^2 = \frac{1}{2}Z_0 I_b^2 \end{aligned} \quad (24)$$

and the power delivered to the matched loads is found using (15) and (21)

$$\begin{aligned} P_{\text{out},3} &= \frac{1}{2}Z_0|I_3|^2 = 0 \\ P_{\text{out},1} &= \frac{1}{2}Z_0|I_1|^2 = Z_0 I_b^2. \end{aligned} \quad (25)$$

As we can see, the input impedances of the BPA are constant and the power generated by each of the balanced current sources sums in phase at the output.

It may seem that we have taken an unnecessarily complex approach to derive fairly well-known results, however the analysis also allows us to easily evaluate the effects that output load mismatch can have on the active input impedance. Performing the same analysis for $\vec{I}_{\text{P}}$, but setting $Z_{\text{x},1} = Z_{\text{L}}$ instead of Z_0 and keeping $Z_{\text{x},1} = Z_0$ reveals

$$\begin{aligned} \begin{bmatrix} I_3 \\ I_1 \end{bmatrix} &= \begin{bmatrix} j\frac{\sqrt{2}Z_{\text{L}}}{Z_0+Z_{\text{L}}} & \frac{\sqrt{2}Z_0}{Z_0+Z_{\text{L}}} \\ \frac{\sqrt{2}Z_0}{Z_0+Z_{\text{L}}} & j\frac{\sqrt{2}Z_{\text{L}}}{Z_0+Z_{\text{L}}} \end{bmatrix} \begin{bmatrix} I_b \\ jI_b \end{bmatrix} \\ &= \begin{bmatrix} j\frac{Z_0 - Z_{\text{L}}}{Z_0+Z_{\text{L}}}\sqrt{2}I_b \\ \frac{\sqrt{2}Z_0}{Z_0+Z_{\text{L}}}\sqrt{2}I_b \end{bmatrix}. \end{aligned} \quad (26)$$

The output load mismatch also affects the active input impedances of ports 2 and 4

$$\begin{aligned} Z_{\text{A},2} &= Z_0\frac{3Z_{\text{L}} - Z_0}{Z_0 + Z_{\text{L}}} = Z_0(1 - 2\Gamma_{\text{L}}) \\ Z_{\text{A},4} &= Z_0\frac{3Z_0 - Z_{\text{L}}}{Z_0 + Z_{\text{L}}} = Z_0(1 + 2\Gamma_{\text{L}}), \end{aligned} \quad (27)$$

which reveals that both devices mismatch in opposite trajectories along the Smith chart [20]–[22]. Figure 4 shows the reflection coefficient seen by the two balanced devices when $Z_{\text{L}} = 25\ \Omega$. The device at port 2 sees $Z_{\text{A},2} \approx 16.7\ \Omega$ and the device at port 4 sees $Z_{\text{A},4} \approx 83.3\ \Omega$. Similarly, when $Z_{\text{L}} = 100\ \Omega$ then $Z_{\text{A},2} \approx 83.3\ \Omega$ and $Z_{\text{A},4} \approx 16.7\ \Omega$.

A more insightful conclusion is that one of the individual active devices within the BPA sees a greater VSWR mismatch than if it were directly connected to Z_{L} [21]. For this reason, asymmetrically tuning the two active devices helps with restoring the VSWR and bandwidth performance of the BPA [22].

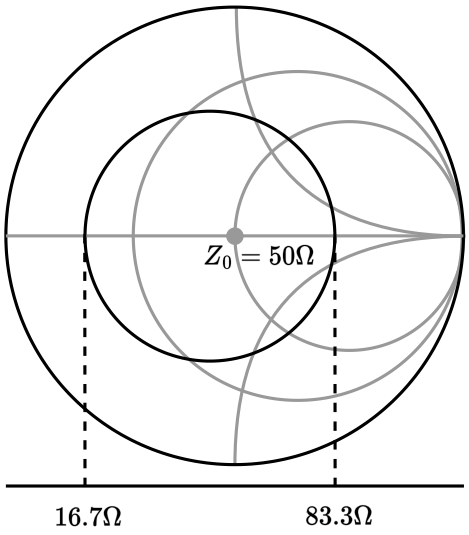

Fig. 4. Reflection coefficient seen by both active devices when $Z_L = 25$.

Example 2: Load-Modulated Balanced Amplifier

As a second example we consider the active input impedance equations of the LMBA. It is a variation of the conventional quadrature hybrid BPA wherein the input impedances seen by both active devices are actively load-modulated by means of a small control signal injected into the isolated port of the BPA. The allows the LMBA to dynamically present the optimum loads to the active devices, allowing them to maintain good efficiency as their output backoff levels vary. Another remarkable result is that the control power used to achieve the tuning is fully recovered at the output, making the LMBA a very efficient system.

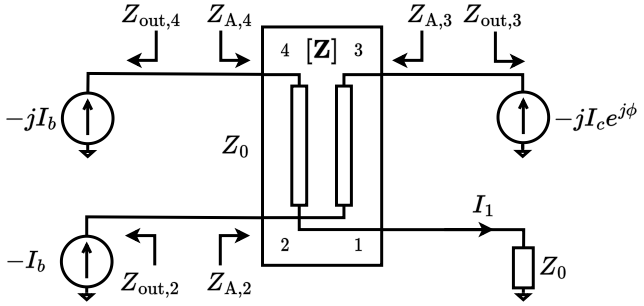

Fig. 5. Conventional LMBA configuration. The active devices are visualized as current sources with a finite output impedance Z_{out}.

We show that deriving the LMBA load-modulation equations becomes straightforward using this technique, unlike previous derivations, e.g. [23]–[26]. Figure 5 shows the output part of the conventional LMBA circuit [5], consisting of an ideal 3dB quadrature hybrid coupler and a matched load. The 4-port Z-matrix of the ideal 3dB hybrid together with its current and voltage relations is

$$Z_0 \begin{bmatrix} 0 & 0 & j & -j\sqrt{2} \\ 0 & 0 & -j\sqrt{2} & j \\ j & -j\sqrt{2} & 0 & 0 \\ -j\sqrt{2} & j & 0 & 0 \end{bmatrix} \begin{bmatrix} I_1 \\ I_2 \\ I_3 \\ I_4 \end{bmatrix} = \begin{bmatrix} V_1 \\ V_2 \\ V_3 \\ V_4 \end{bmatrix}. \quad (28)$$

The two balanced devices are represented by current sources, having equal magnitude I_b with a quadrature phase offset, and are connected to ports 2 and 4, such that $I_2 = -I_b$ and $I_4 = -jI_b$, respectively. The control signal has a variable magnitude, I_c, and phase offset relative to I_b, ϕ, and is injected in port 3, such that $I_3 = -jI_c e^{j\phi}$. Thus, we define the passive and active current vectors as

$$\vec{i_{\text{P}}} = \begin{bmatrix} I_1 \end{bmatrix} \text{ and } \vec{i_{\text{A}}} = \begin{bmatrix} I_2 \\ I_3 \\ I_4 \end{bmatrix} = \begin{bmatrix} -I_b \\ -jI_c e^{j\phi} \\ -jI_b \end{bmatrix}. \quad (29)$$

Port 1 is connected to a matched load, such that $\vec{z}_x = [Z_{x,1}] = [Z_0]$, and the normalized loading matrix is

$$\mathbf{X} = \frac{1}{Z_0}\begin{bmatrix} Z_0 \end{bmatrix} = [1]. \quad (30)$$

The impedance matrix $\mathbf{Z}$ is rearranged and partitioned in the following manner

$$\begin{aligned} \mathbf{A} &= \begin{bmatrix} 0 \end{bmatrix} \\ \mathbf{B} &= \begin{bmatrix} 0 & j & -j\sqrt{2} \end{bmatrix} \\ \mathbf{C} &= \begin{bmatrix} 0 \\ j \\ -j\sqrt{2} \end{bmatrix} \\ \mathbf{D} &= \begin{bmatrix} 0 & -j\sqrt{2} & j \\ -j\sqrt{2} & 0 & 0 \\ j & 0 & 0 \end{bmatrix} \end{aligned} \quad (31)$$

Using equation (8) we are able to compute the current flowing through the output load

$$I_1 = \begin{bmatrix} 0 & j & -j\sqrt{2} \end{bmatrix} \begin{bmatrix} -I_b \\ -jI_c e^{j\phi} \\ -jI_b \end{bmatrix} = I_c e^{j\phi} + \sqrt{2} I_b, \quad (32)$$

meaning both the balanced and control currents are fully recovered at port 1. The voltages $\vec{v}_{\text{A}}$ across the active ports are evaluated using (9), giving us

$$\vec{v_{\text{A}}} = Z_0 \begin{bmatrix} 0 & -j\sqrt{2} & \sqrt{2}j \\ -j\sqrt{2} & 1 & \sqrt{2} \\ j & \sqrt{2} & 2 \end{bmatrix} \begin{bmatrix} -I_b \\ -jI_c e^{j\phi} \\ -jI_b \end{bmatrix}. \quad (33)$$

Finally, the active input impedance $\vec{z}_{\text{A}}$ can be solved using (10), giving us the familiar LMBA input impedance equations for the active ports

$$\begin{aligned} Z_{\text{A},2} &= Z_0 \left(1 + \sqrt{2}\frac{I_c}{I_b} e^{j\phi}\right) \\ Z_{\text{A},3} &= Z_0 \\ Z_{\text{A},4} &= Z_0 \left(1 + \sqrt{2}\frac{I_c}{I_b} e^{j\phi}\right). \end{aligned} \quad (34)$$

The input impedances $Z_{\text{A},2}$ and $Z_{\text{A},4}$ are identical and can be actively load-modulated by adjusting the magnitude and phase of the control current $I_c e^{j\phi}$ relative to the balanced current I_b. Conversely, the input impedance $Z_{\text{A},3}$ remains

constant and is not affected by any load-modulation. Figure 6 illustrates the range of complex impedances that can be actively load-modulated with a conventional LMBA where the control power does not exceed the power of a single balanced device. It is worth noting that these relations hold true as long as the load impedance is $Z_{x,1} = Z_0$.

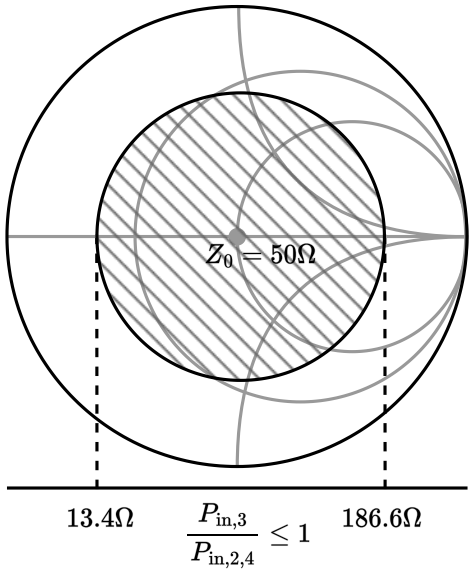

Fig. 6. Region of achievable load-modulated impedances for the conventional LMBA.

The power generated by each current source $\vec{I}_A$ is found using (14)

$$\begin{aligned} P_{in,2} &= \frac{1}{2} Z_0 \left(I_b^2 + \overline{2} I_b I_c \cos\phi \right) \\ P_{in,3} &= \frac{1}{2} Z_0 I_c^2 \\ P_{in,4} &= \frac{1}{2} Z_0 \left(I_b^2 + \overline{2} I_b I_c \cos\phi \right) \end{aligned} \tag{35}$$

and, using (15), the power delivered to the output load is

$$P_{out,1} = Z_0 \left(I_b^2 + \overline{2} I_b I_c \cos\phi + \frac{1}{2} I_c^2 \right), \tag{36}$$

all of which is in complete agreement with the results from [5] and confirms the power conservation property of the LMBA design.

The analysis also allows direct evaluation of the effect the output loads $\vec{Z}_x$ can have on the input impedances of the active ports. Performing the same analysis for the LMBA, but setting $Z_{x,1} = Z_L$ instead of Z_0 yields

$$\begin{aligned} Z_{A,2} &= Z_0 \left(1 + \overline{2} \frac{I_c}{I_b} e^{j\phi} \right) \\ Z_{A,3} &= Z_0 \left(\frac{Z_0}{Z_L} + \left(\frac{Z_0 \quad Z_L}{Z_L} \right) \overline{2} \frac{I_b}{I_c} e^{\quad j\phi} \right) \\ Z_{A,4} &= Z_0 \left(\frac{2Z_0 \quad Z_L}{Z_L} + \frac{Z_0}{Z_L} \overline{2} \frac{I_c}{I_b} e^{j\phi} \right). \end{aligned} \tag{37}$$

The equations reveal that the LMBA behaviour is susceptible to output load mismatch, such as antenna loading, highlighting the challenging MIMO environments [10]. The load mismatch causes the input impedances at ports 2 and 4 to no longer be identical and also introduces active load-modulation at port 3, with the control current I_c in the denominator, which may affect the power conservation properties. If $I_c < I_b$ the fraction can become much greater than unity and as a consequence $Z_{A,3}$ can become vastly different than Z_0, and even negative. For example, if $Z_L = 2Z_0$ and $I_b/I_c e^{j\phi} = \quad 2$, then $Z_{A,3} \quad 1.9Z_0$. Similarly, if $Z_L = Z_0/2$ and $I_b/I_c e^{j\phi} = \quad 2$, then $Z_{A,3} \quad 0.83Z_0$, which may lead to instability and even damage the control device. Our analysis can help determine practical constraints w.r.t. load mismatch and required I_c. Note that when $Z_L = Z_0$, (25) reduces to (22).

C. Unique Hybrid Coupler Arrangements

As shown by the two examples, the presented technique offers a systematic approach to solving the active input impedance and current relations for a given network. It opens the way to systematically evaluate existing, as well as new, system designs; to explore their behaviour under mismatch conditions and to develop clearer insights into their performance limits. We have limited the scope of examples to the quadrature hybrid coupler only, because it can still reveal surprising results, despite its long history. There exist several system configurations which incorporate a hybrid coupler and active devices, such as BPAs, diode linearizers (DL), LMBAs, and many others. By understanding how multiple active devices interact through a network we can gain further design insights and recognise that they share common boundaries and constraints.

For example, in the conventional BPA hybrid coupler architecture, under ideal conditions, the two active devices are designed to have constant output impedance ($Z_{out} = Z_0$) just as the hybrid's input impedances are fixed ($Z_{A,2,4} = Z_0$). This results in all the currents summing constructively at the output port and no current flows from the isolated port ($jI_3j = 0$). Diode linearisers, on the other hand, rely on two actively biased diodes with a nonlinear current-dependent variable output impedance (ideally on the edge of the Smith chart) which cause a mismatch between the coupler's fixed input impedance ($Z_{A,2,4} = Z_0$) to correct for AM/PM distortion in a lossless manner ($jI_3j = jI_{2,4}j$). The LMBA, as already explained, uses a small control signal ($jI_3j < jI_{2,4}j$) to actively tune the input impedances of the hybrid coupler ($Z_{A,2,4} \;/\; Z_0 \frac{I_3}{I_{2,4}}$ for brevity), to match the varying output impedances of the active devices, thus maintaining good efficiency at varying backoff levels and even recovering the control signal.

Thus, an active device can either be designed to have a constant or varying output impedance and a network can either have a fixed or tunable input impedance. Table I summarizes the classifications between all the above-mentioned devices. And what of the upper right quadrant where the input impedances of the hybrid can be actively tuned, while the output impedances of the active devices is kept constant? This configuration results in a device, which we have named the Load-Modulated Linearizer (LML), that is able to correct

TABLE I
CURRENT BOUNDARY CONDITIONS FOR EVERY KIND OF AMPLIFIER AND LINEARISER DEVICE IMPLEMENTED USING SOME 4-PORT HYBRID.

Variable Output Impedance \ Tunable Input Impedance		Constant Output Impedance \ Fixed Input Impedance
LMBA: 1) $Z_{A,2,4} \;/\; Z_0 \frac{I_3}{I_{2,4}}$ 2) $\lvert I_3\rvert < \lvert I_{2,4}\rvert$	LML: 1) $Z_{A,2,4} \;/\; Z_0 \frac{I_3}{I_{2,4}}$ 2) $\lvert I_3\rvert > \lvert I_{2,4}\rvert$	
DL: 1) $Z_{A,2,4} = Z_0$ 2) $\lvert I_3\rvert = \lvert I_{2,4}\rvert$	BPA: 1) $Z_{A,2,4} = Z_0$ 2) $\lvert I_3\rvert = 0$	

AM/AM distortion at high PA compression levels by actively controlling the input impedance matching between its active devices and the coupler. The roles of the control and balanced currents are interchanged, in contrast to the LMBA ($|I_3| > |I_{2,4}|$).

III. LOAD-MODULATED LINEARIZATION THEORY

Active load-modulation can emulate impedances within and beyond the boundary of the Smith chart. This opens the possibility to selectively absorb undesired signals, such as OOB IMD products, while leaving other signals unaffected independent of the frequency spacing between them [11]. We refer to this process as load-modulated linearization and the LMBA architecture is a suitable platform for developing this concept due to its three key characteristics:

1) Input impedances at ports 2 and 4 can be actively tuned,
2) The input impedance of port 3 remains fixed at Z_0,
3) The control power is fully recovered at port 1.

In the conventional LMBA arrangement the control current enters port 3 and the main currents, generated by the two balanced devices, enter ports 2 and 4, as already shown in Fig. 5. The control current should not exceed the balanced current, by definition, which limits the range of values that the input impedances of ports 2 and 4 can be actively load-modulated to. We propose a different arrangement called the Load-Modulated Linearizer (LML), where the current I_{in} is generated by a main device at port 3 and the currents $I_c e^{j\phi}$ are generated by two control devices at ports 2 and 4, respectively. In this manner we are able to achieve much greater load-modulation ranges than the LMBA using very low control power. The topology of the proposed load-modulating linearization system is shown in Fig. 7.

The input impedance expressions for ports 2 and 4 remain the same as for the regular LMBA case, except that the roles of the main and control PAs have been reversed, so we introduce the following simplified notation

$$Z_{\text{A}} = Z_{\text{A},2,4} = Z_0 \left(1 + \sqrt{2}\frac{I_{\text{in}}}{I_c} e^{\;j\phi}\right), \tag{38}$$

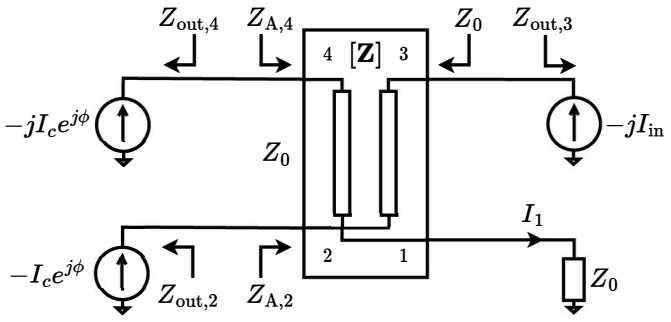

Fig. 7. Topology of the proposed LML system. The main current, I_{in}, enters port 3 and interacts with the control currents.

which can achieve a greater load-modulation range than the LMBA by keeping the magnitude of the control current I_c smaller than I_{in}, which is quite convenient. The input impedance at port 3 is Z_0 and is not affected by load-modulation under matched load conditions. The sum total input power, which can be spread across some bandwidth, is

$$P_{\text{in}} = \frac{1}{2} Z_0 |I_{\text{in}}|^2 \tag{39}$$

and the control power entering ports 2 and 4 is

$$2P_{\text{C}} = \text{Re}\{Z_{\text{A}}\} |I_c|^2 = Z_0 \left(I_c^2 + \sqrt{2} I_{\text{in}} I_c \cos\phi\right). \tag{40}$$

The total output power P_{out} delivered into the matched output load from port 1 thus becomes

$$\begin{aligned} P_{\text{out}} &= 2P_{\text{C}} + P_{\text{in}} = \left(\frac{2+\alpha}{\alpha}\right) P_{\text{in}} \\ &= \frac{|Z_{\text{A}}/Z_0 \quad 1|^2 + 4\,\text{Re}\{Z_{\text{A}}/Z_0\}}{|Z_{\text{A}}/Z_0 \quad 1|^2} P_{\text{in}} \\ &= \left|\frac{Z_{\text{A}}/Z_0 + 1}{Z_{\text{A}}/Z_0 \quad 1}\right|^2 P_{\text{in}}, \end{aligned} \tag{41}$$

where we have used $4\,\text{Re}\{Z_{\text{A}}/Z_0\} = |Z_{\text{A}}/Z_0 + 1|^2 - |Z_{\text{A}}/Z_0 \quad 1|^2$. The factor $2P_{\text{C}}$ reflects that there are two control devices and the factor α is the ratio between the input and control power which is found using (40)

$$\begin{aligned} \alpha = \frac{P_{\text{in}}}{P_{\text{C}}} &= \frac{P_{\text{in}}}{P_{\text{av-C}}(1 \quad |\Gamma_{\text{A}}|^2)} = \frac{\frac{1}{2} Z_0 |I_{\text{in}}|^2}{\frac{1}{2}\text{Re}\{Z_{\text{A}}\} |I_c|^2} \\ &= \frac{\left|\frac{Z_{\text{A}}/Z_0 \quad 1}{\sqrt{2}}\right|^2 |I_c|^2}{\text{Re}\{Z_{\text{A}}/Z_0\} |I_c|^2} = \frac{|Z_{\text{A}}/Z_0 \quad 1|^2}{2\text{Re}\{Z_{\text{A}}/Z_0\}}, \end{aligned} \tag{42}$$

with $P_{\text{av-C}}$ being the maximum available control power (for a given bias) from a single control device. The active reflection coefficient Γ_{A} for both ports 2 and 4 affects how much of $P_{\text{av-C}}$ can be delivered into the output hybrid coupler

$$\Gamma_{\text{A}} = \Gamma_{\text{A},2,4} = \frac{Z_{\text{A}} \quad Z_{\text{out}}}{Z_{\text{A}} + Z_{\text{out}}}. \tag{43}$$

The output power P_{out} is highest when the input impedances Z_{A} of the coupler are conjugately matched to the output

impedance of the active device ($Z_{\mathrm{A}} = Z_{\mathrm{out}}$), which guarantees maximum power transfer, such that $P_{\mathrm{C}} = P_{\text{av-C}}$.

By definition, factor α is constrained to real values, however there are no constraints on whether these values can be negative or positive. While it may seem counter-intuitive for a power ratio to be negative, we note that since we can modulate Z_{A} to negative resistances, i.e. $\mathrm{Re}\{Z_{\mathrm{A}}\} < 0$, we can also achieve an active input reflection coefficient $|\Gamma_{\mathrm{A}}|^2 > 1$ from the perspective of the available control power delivered to the hybrid coupler. In other words, power can be made to flow either in or out of ports 2 and 4, despite the presence of active devices.

The LML can operate like an LMBA and couple all input power, along with the control power, to the output load by setting $Z_{\mathrm{A}} = Z_{\mathrm{out}}$. And as will be shown later, the closer Z_{out} is to the Smith chart's edge, the greater α is, and the less available control power is needed for load-modulation. This is a direct result of Eq. (38), which allows for $\alpha \geq 1$ while the LMBA is constrained to $0 \leq \alpha \leq 1$. Alternatively, the LML can fully prevent any input power from reaching the output load at port 1 by means of setting $Z_{\mathrm{A}} = Z_0$ such that $\alpha = 2$, which is achieved by maintaining an amplitude and phase relation $I_c e^{j\phi} = I_{\mathrm{in}}/\sqrt{2}$ in Eq. (38). This results in $P_{\mathrm{out}} = 0$ for any P_{in} from Eq. (41), and as $Z_{\mathrm{A},3} = Z_0$, there are no stability concerns for the main PA. Thus, the LML has the ability to selectively couple input power at given frequencies and absorb input power at other frequencies, making it e.g. very suitable for cancelling distortion products and harmonics without affecting the main tones. The active input impedances that the control devices must see in order to either couple or absorb power become

$$Z_{\mathrm{A}} = \begin{cases} Z_{\mathrm{out}} & \text{for all wanted power} \\ Z_0 & \text{for all unwanted power.} \end{cases} \tag{44}$$

With the active input impedance constraints in place we can define the necessary conditions and available control power requirements for both coupling the input power we consider desired and absorbing all other power, such as IMD products and harmonics.

So far we have referred to the input power as simply P_{in} in order to more clearly express the power conservation properties which the LML inherits from the LMBA. We now define the input power as the linear sum (no spectral overlap) of the sum total main power P_{M} and sum total distortion power P_{M}

$$P_{\mathrm{in}} = P_{\mathrm{M}} + P_{\mathrm{D}}. \tag{45}$$

The goal of the LML is to losslessly couple all P_{M} to the output load while, simultaneously, absorbing all unwanted P_{D}. In the following subsections we will present the necessary conditions for achieving both tasks.

A. Control Power Required for Coupling

In order to couple all P_{M} losslessly to the output port we need to modulate Z_{A} to Z_{out}. The amount of available control power, $P_{\text{av-C}j\mathrm{M}}$, required is found by rearranging Eq. (42)

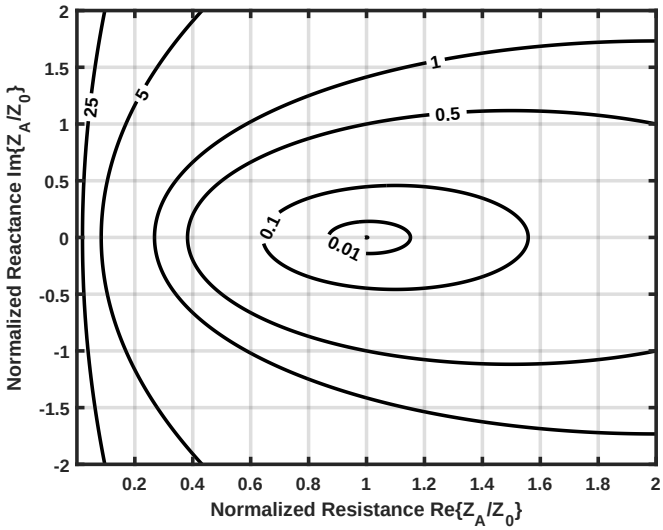

Fig. 8. Contour plot of positive α values w.r.t. real and imaginary normalized impedance Z_{A}/Z_0 and $\mathrm{Re}\{Z_{\mathrm{A}}/Z_0\} > 0$.

$$P_{\text{av-C}j\mathrm{M}} = \frac{2\mathrm{Re}\{Z_{\mathrm{out}}/Z_0\}}{|jZ_{\mathrm{out}}/Z_0 - 1|^2} P_{\mathrm{M}} = \frac{P_{\mathrm{M}}}{\alpha}. \tag{46}$$

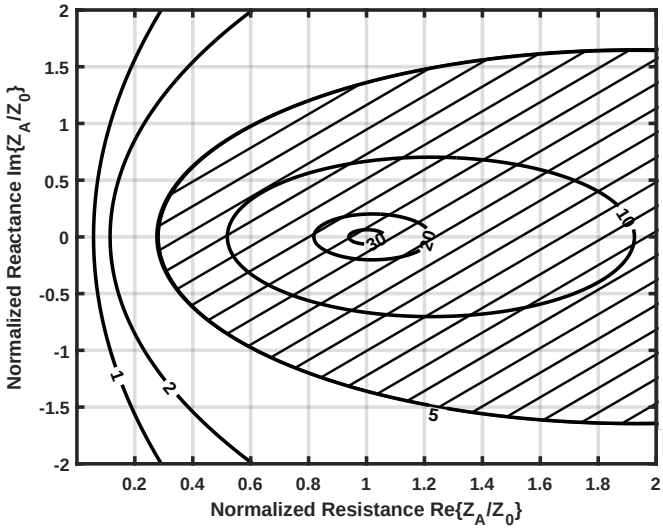

Fig. 9. Contour plot of output power P_{out} in dBc as a function of Z_{A}/Z_0 when coupling power. The shaded region is infeasible for the LML as $\alpha \geq 1$.

Figure 8 shows a Cartesian contour plot of positive α values as a function of normalised impedance Z_{A}/Z_0 for $\mathrm{Re}\{Z_{\mathrm{A}}/Z_0\} > 0$. The amount of $P_{\text{av-C}j\mathrm{M}}$ necessary to load-modulate Z_{A} to Z_{out} decreases to zero when Z_{out} becomes a fully reactive load. Conversely, more $P_{\text{av-C}j\mathrm{M}}$ is necessary when Z_{out} converges to Z_0. When $\alpha < 1$, the available control power exceeds the main power in order to maintain $Z_{\mathrm{A}} = Z_{\mathrm{out}}$, and since the control power is fully recovered, the output power P_{out} begins to increase as well, as described by Eq. (41). Figure 9 shows the contour plot of P_{out} as a function of normalised impedance Z_{A}/Z_0 for $\mathrm{Re}\{Z_{\mathrm{A}}/Z_0\} > 0$. When $Z_{\mathrm{A}} = Z_0$ the output power becomes infinite, since the control devices must deliver infinite power, which is not considered good design

practice. It is for this reason that the LML is restricted to α 1, as shown by the shaded area in Fig. 9.

B. Control Power Required for Absorbing

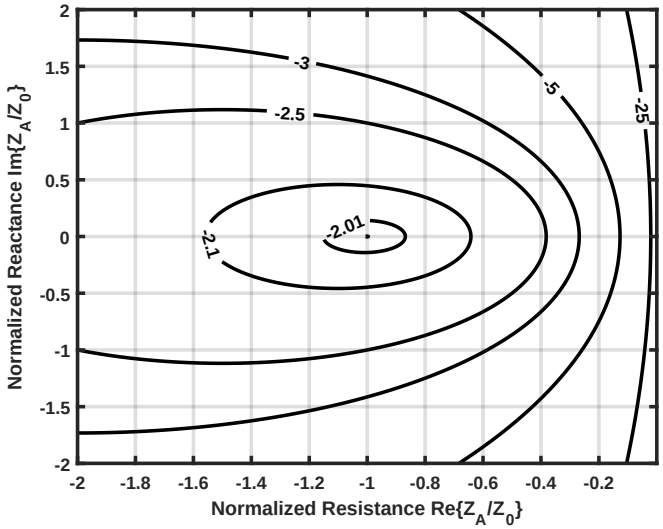

Fig. 10. Contour plot of negative values w.r.t. real and imaginary normalized impedance Z_A/Z_0 and $\mathrm{Re}\{Z_A/Z_0\} < 0$.

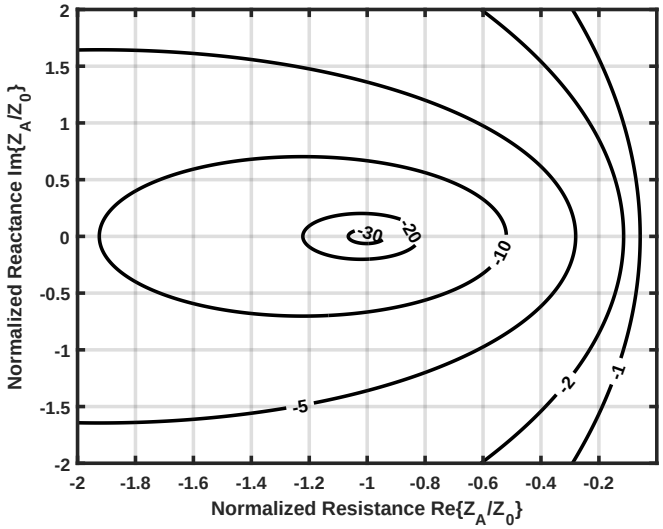

Fig. 11. Contour plot of output power P_{out} in dBc as a function of Z_A/Z_0 when absorbing power.

Similarly, In order to absorb all P_D into the control PAs we need to modulate Z_A to Z_0. The amount of available control power, $P_{\text{av-C}jD}$, required is found by combining Eqs. (42) and (43)

$$P_{\text{av-C}jD} = \frac{P_D}{2(1 \quad j \quad _A j^2)} = \frac{jZ_{out}/Z_0 \quad 1j^2}{8\mathrm{Re}\{Z_{out}/Z_0\}} P_D = \frac{\alpha}{4} P_D. \quad (47)$$

Figure 10 shows a Cartesian contour plot of negative α values as a function of normalized impedance Z_A/Z_0 for $\mathrm{Re}\{Z_A/Z_0\} < 0$. The largest negative value that α can achieve is 2 and combining with Eq. (41), guarantees that no distortion power will reach the output port. The amount of $P_{\text{av-C}jD}$ necessary to load-modulate Z_A to Z_0 decreases to zero when Z_{out} becomes Z_0, as that implies a perfect match at ports 2 and 4. Conversely, more $P_{\text{av-C}jD}$ is necessary when Z_{out} becomes a fully reactive load. Figure 11 shows the contour plot of P_{out} as a function of normalised impedance Z_A/Z_0 for $\mathrm{Re}\{Z_A/Z_0\} < 0$. When $Z_A = Z_0$ the output power becomes zero, since the control devices absorb all the distortion power, leaving no remaining control power. This effect is achieved only when $\alpha = 2$.

C. Load-Modulation Solution Space

Figure 12 is a 3D Smith chart (or Smith sphere) [27], which is a convenient way to associate the α values necessary to load-modulate the drive impedance Z_A to any point within the complex impedance plane for some non-zero P_{in}. The northern hemisphere is a projection of the familiar (2D) Smith chart. Here all complex impedances have a non-negative real part and all α 0, meaning that modulated Z_A values in this region will result in some power coupling to the output. The north pole represents a perfect match ($Z_A/Z_0 = 1$) and $\alpha = 0$ and reaching it requires $P_{\text{av-C}}/P_{in}$! 1 . Load-modulating towards the northern voltage standing wave ratio (VSWR) parallel, bound by $\alpha = 1$, requires $P_{\text{av-C}} = P_{in}$. The equatorial VSWR parallel represents purely reactive loads, for which α tends to 1 depending on whether the equator is approached from the north or the south, respectively. When coupling, reaching the equator does not require any $P_{\text{av-C}}$. The contour plot of Fig. 8 is a linear projection of the northern hemisphere, where the circular parallels of the Smith sphere become ellipses [27].

The southern hemisphere contains all complex impedances that have negative real part and all α 2, meaning power absorption is possible. The southern VSWR parallel bound by $\alpha = 3$ requires $P_{\text{av-C}} = P_{in}/3$. Consequently, power absorption is not optimal as the output power at port 3 will be $P_{out} = P_{in}/3$. Finally, the south pole represents a perfect anti-match ($Z_A/Z_0 = 1$) and $\alpha = 2$, and reaching it requires $P_{\text{av-C}} = P_{in}/2$ from Eq. (45), which is the optimal condition for absorbing all unwanted power. The contour plots of Figs. 10 is also a linear projection of the southern hemisphere, in which the circular parallels of the Smith sphere also become ellipses [27].

D. Minimum Control Power

Equations (46) and (47) reveal that the coupling and absorption mechanisms oppose each other with regards to choice of Z_{out}. The coupling mechanism requires no control power when Z_{out} is purely reactive and an infinite amount of control power when the control PA's output impedance becomes Z_0. Conversely, the absorption mechanism requires no control power when $Z_{out} = Z_0$ and an infinite amount of control power when Z_{out} becomes purely reactive.

The total available control power, $P_{\text{av-C}jT}$, necessary to achieve both coupling and absorption with respect to Z_{out} is

$$P_{\text{av-C}jT} = P_{\text{av-C}jM} + P_{\text{av-C}jD}, \quad (48)$$

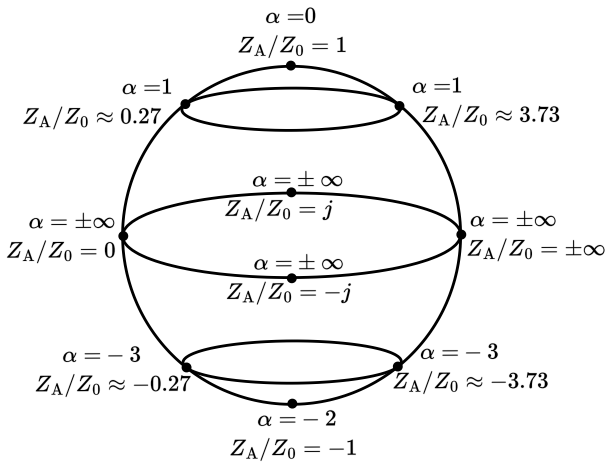

Fig. 12. Smith sphere representing the complex impedance space for normalized drive impedance Z_A=Z_0 and the corresponding values of .

which can be rearranged using (46) and (47) in terms of α such that

$$P_{\text{av-C}j\text{T}} = \frac{P_\text{M}}{\alpha} + \frac{\alpha}{4}P_\text{D}. \tag{49}$$

This relation is valid only when the conditions of Eq. (44) are met. By separating the main PA's output into P_M and P_D we can determine an optimal Z_out between the two load-modulation mechanisms such that the least amount of control power is necessary to satisfy both

$$\frac{\mathrm{d}}{\mathrm{d}\alpha}P_\text{T} = -\frac{P_\text{M}}{\alpha^2} + \frac{P_\text{D}}{4} = 0, \tag{50}$$

for which the optimum occurs when

$$\alpha = 2\sqrt{\frac{P_\text{M}}{P_\text{D}}}. \tag{51}$$

This result allows us to relate Z_out directly to P_M and P_D. Direct substitution of the optimum α in Eq. (49) allows us to determine the minimum necessary available control powers

$$P_{\text{av-C}j\text{M}} = P_{\text{av-C}j\text{D}} = \frac{1}{2}\sqrt{P_\text{M}P_\text{D}}. \tag{52}$$

This remarkable result shows that the required available control power necessary to fully couple every tone that is part of the main output power coming out of the main device to the output port is equal to the available control power necessary to fully absorb every distortion tone and that both amounts are entirely determined by the total amount of main and distortion power. The minimum available control power per device necessary to both couple and absorb a given amount of wanted and unwanted power is simply the geometric mean of the total main and total distortion powers

$$P_{\text{T-min}} = \sqrt{P_\text{M}P_\text{D}}. \tag{53}$$

E. Optimum Control Device Output Impedance

Thus, P_M and P_D uniquely determine the optimum Z_out at which coupling and absorption can be achieved using the least available total control power. A compact solution for a purely real Z_out is

$$Z_\text{out}/Z_0 = \frac{1 \quad \sqrt{\frac{\alpha}{2+\alpha}}}{1 \quad \sqrt{\frac{\alpha}{2+\alpha}}}, \tag{54}$$

whose values define a VSWR circle w.r.t. Z_0, which also contains all complex solutions as already illustrated in Fig. 12. If the VSWR circle intersects the real axis of the Smith chart at, e.g. 8.58 or 291.42 , then all impedances which lie on the circle will produce the same α, e.g., Z_out = 9.5 + j16.1 .

As a broader example, when the main device operates in compression and amplifies two tones each at 30dBm, the resulting sum total main power is P_M = 33dBm. Consequently, several IMD tones emerge across the spectrum whose sum total is assumed here to be P_D = 13dBm. Using (51) we find that α = 20 and the optimum output impedance that the control devices must have is a VSWR circle which intersects the real axis of the Smith chart at approximately 1.2 . The minimum available control power per control device necessary to couple all P_M and absorb all P_D becomes $P_{\text{T-min}}$ = 23dBm with $P_{\text{av-C}j\text{M}}$ = $P_{\text{av-C}j\text{D}}$ = 20dBm. The control devices need to deliver 10dB less power than the main device, allowing them to remain significantly linear. The control power used to couple every main tone to the output is also conserved (α = 20), so P_out = 33.4dBm.

Figure 13 shows the amount of available control power that each control device must deliver in order to couple a reference P_M power and absorb a relative P_D power (dBc) as a function of Z_out in a 50 environment. The output impedance is shown only as real for the sake of clarity. The $P_{\text{T-min}}$ curve shows the minimum available control power as P_D increases.

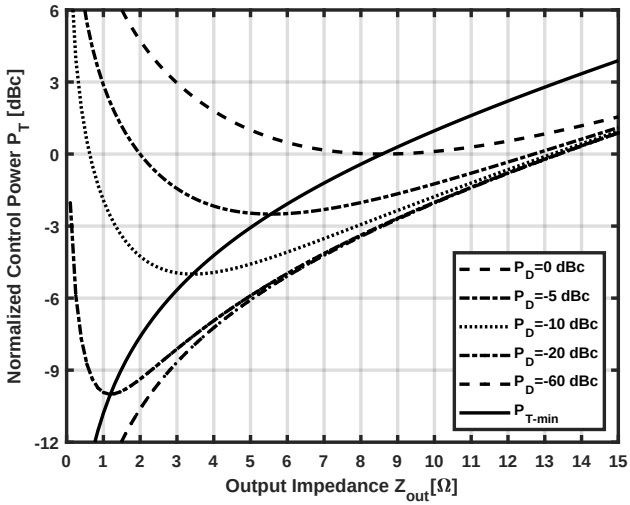

Fig. 13. Relative total control power from a single control PA necessary to couple a reference $P_\text{M}$and absorb different relative amounts of P_D as a function of Z_out. The $P_{\text{T-min}}$ curve shows the minimum relative available control power.

F. System Efficiency

The overall system efficiency, η_{LML}, is defined as the ratio between useful output RF power, $\text{P}_{\text{RF,out}}$, and total DC power, $\text{P}_{\text{DC,total}}$, under the condition that the system operates at minimum control power. So,

$$\eta_{\text{LML}} = \frac{\text{P}_{\text{RF,out}}}{\text{P}_{\text{DC,total}}} = \frac{\left(\frac{\alpha+2}{\alpha}\right) P_{\text{M}}}{\frac{P_{\text{in}}}{\eta_{\text{M}}} + \frac{2P_{\text{T-min}}}{\eta_{\text{C}}}} = \frac{(P_{\text{M}} + P_{\text{T-min}})\,\eta_{\text{M}}\eta_{\text{C}}}{(P_{\text{M}} + P_{\text{D}})\,\eta_{\text{C}} + 2P_{\text{T-min}}\eta_{\text{M}}}, \tag{55}$$

where η_{M} and η_{C} are the device efficiencies [28] of the main and control devices, respectively. In a real system, the control devices will be sized according to the necessary power for the LML to work at sufficient linearity. Therefore, they are likely to be less efficient than the main PA operating in compression.

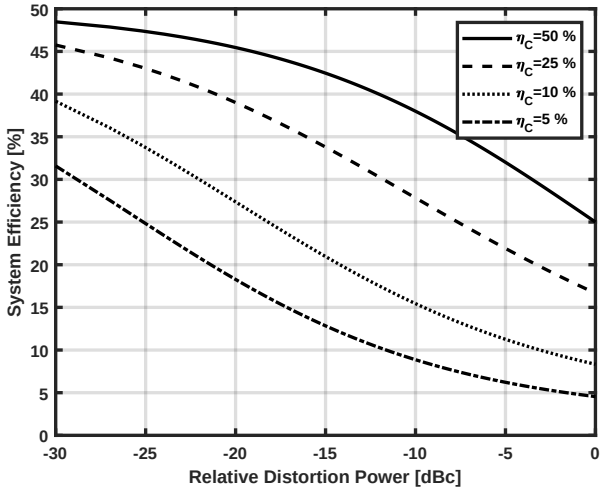

Fig. 14. Total system efficiency as function of increasing relative distortion power P_{D} in dBc for several control device efficiencies. The main device's efficiency is fixed at $_{\text{M}}$ = 50%.

For example, if η_{M} = 50%, η_{C} = 25%, and P_{D} = 20dBc, the total system efficiency would only decrease to 39%, as shown in Fig. 14. As the relative amount of P_{D} increases, the overall system becomes less and less efficient as more $P_{\text{av-C}j\text{D}}$ is necessary to absorb it. High efficiency and low power control devices are particularly useful in this configuration.

IV. Experimental Validation

The topology of the proposed LML system is shown in Fig. 15. It is constructed using three identical commercial PAs (ZRL-2400LN+, 1 2.4GHz) with input-related P_{1dB} = 9dBm and P_{3dB} = 7dBm. The LML consists of two control amplifiers, PA_{C}, whose output impedance Z_{out} is set to 8 (α 2.2) using a pair of custom PCB-based quarter-wave transformers. The main PA, PA_{M}, operates in compression where it is most efficient (drain efficiency η_{M} = η_{C} 4.5% at P_{1dB} and 7% at P_{3dB}) and produces an amount of desired power, P_{M}, and an amount of unwanted distortion power, P_{D}, spread across the bandwidth of interest. The two main input tones, centered at 2GHz, are generated using two signal generators, and the coupling (2) and absorbing (4) control tones are generated using six separate signal generators, which are represented by a single piece of equipment for clarity. Wilkinson combiners (ZN2PD2-63-S+, 0.35 6GHz) are used to guarantee 20dB of isolation between the generators. The combiners and the quadrature hybrid couplers have an insertion loss of approximately 0.9dB each; these losses were compensated for in the generation and it is assumed that Z_{out} is remains sufficiently constant across the bandwidth of operation.

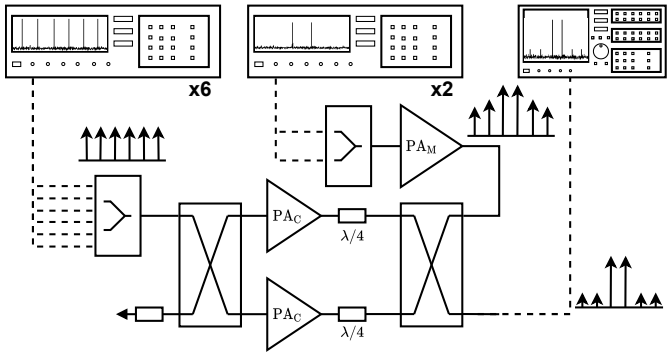

Fig. 15. Measurement setup of LML. The two coupling and four absorbing tones are generated separately using six signal generators on the control side and the two main input tones are generated 100kHz apart on the PA_{M} side using two signal generators.

The PA_{M} is driven at its P_{3dB} compression point by two tones 100kHz apart, producing two main tones as well as several unwanted IMD tones. Once the amplitude of each control tone is evaluated, they are individually phase-shifted until the desired effect is achieved. A suppression of 30dB requires a phase accuracy of 2 degrees and an amplitude accuracy of 0.5dB.

Fig. 16 a) shows the output spectrum of the PA_{M} operating at its P_{3dB} compression point, amplifying two main tones and producing several out of band IMD components, the strongest ones being IM31, IM32, IM51, and IM52. In Fig. 16 b) an overall IMD suppression of about 30dB is measured, while coupling the main tones and their control tones at the output. The slight increase in P_{out} comes from the contribution of the control tones due to α. As an added benefit, tones that are not actively absorbed, such as IM7 and higher order ones (not shown in Fig. 16), experience a passive attenuation of about 3dB, due to Z_{out} = 8 , when they reach the output port.

A. Benchmarking Against DPD

We compare the LML to the simplest form of DPD, implemented as shown in Fig. 17. Two main tones and two IM3 correction tones are generated and combined in the same way as with the LML and are applied to the same PA_{M}.

The output power of the LML and DPD systems is compared to that of the main PA's P_{M} as a function of input power and the results are shown in Figs. 18a) and b). The LML maintains a constant relative power increase over PA_{M} due to the contribution of the control PAs, whereas the DPD system, due to its different nature, incurs a certain power cost from the

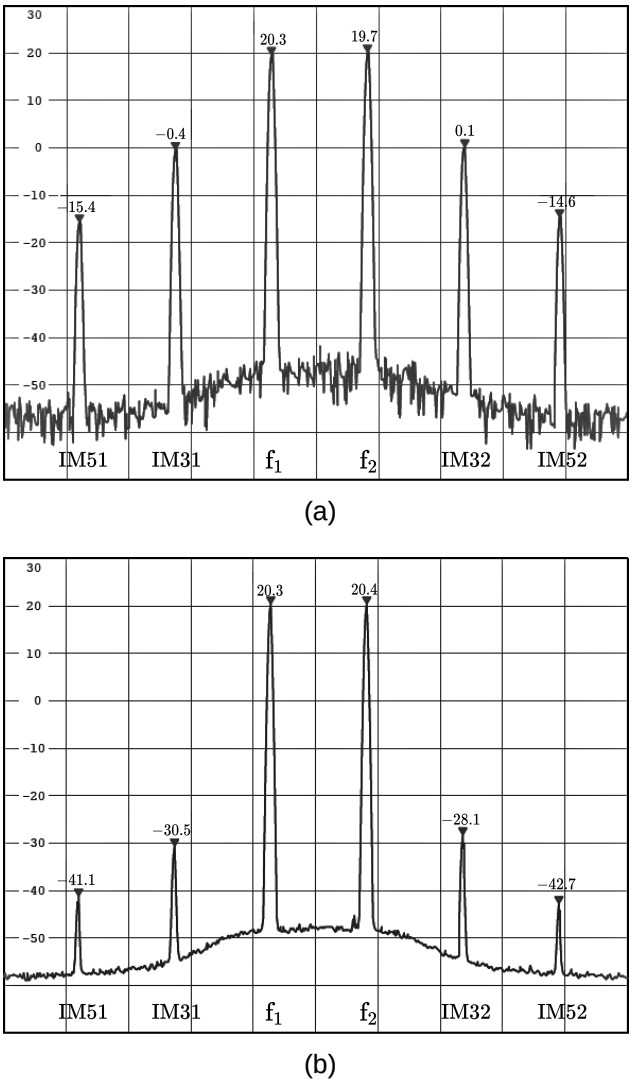

Fig. 16. Output spectrum of the PA_M operating at P_{3dB} for (a) PA_M output and (b) LML output. The spectrum shown in (b) is averaged to better illustrate the amount of achieved suppression.

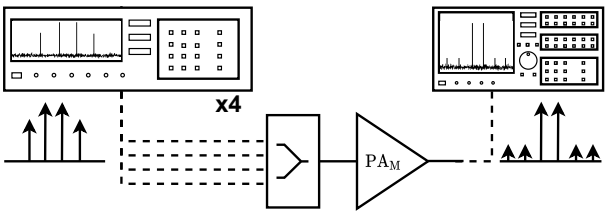

Fig. 17. Measurement setup of DPD with two main tones and two correction tones generated 100kHz apart.

correction tones. The LML does not restrict the output power as the input power is increased past the P_{1dB} compression point. On the other hand, the DPD system causes an eventual gain compression as suppressing the growing IM3 products requires a corresponding (exploding) power increase in the correction tones.

In a similar manner, the suppression of the IM3 tones is compared between the LML and DPD in Figs. 18c) and d). Both the LML and DPD are about equally sensitive to

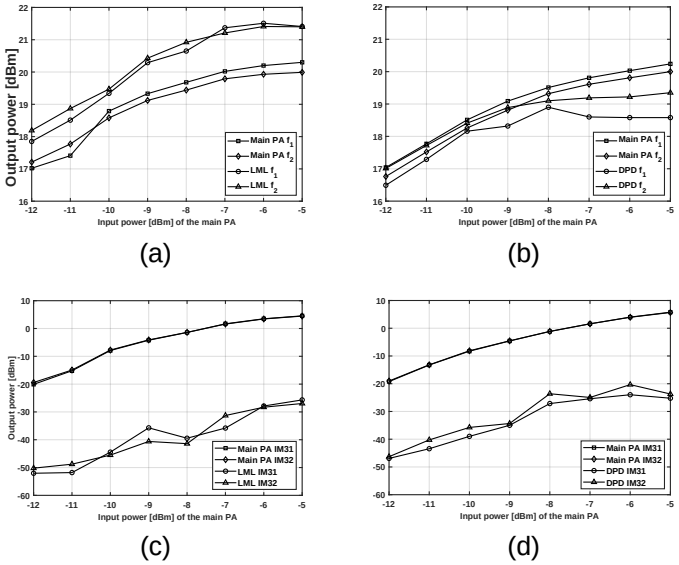

Fig. 18. Output power of LML and DPD systems relative to PA_M's output power for a range of input powers. (a) Output tones of PA_M and LML. (b) Output tones of PA_M and DPD. (c) IM3 tones of PA_M and LML. (d) IM3 tones of PA_M and DPD.

amplitude and phase errors in the control and correction tones, respectively, but the LML does not influence the behaviour of IMD the same way DPD does. The two systems are able to suppress the IM3 tones about equally well, however, the LML can selectively absorb individual unwanted tones and requires simpler control signals, which also simplifies the necessary control scheme.

We compare the sensitivity of the LML and DPD systems to amplitude and phase variations in the absorption control tones. First, the main PA is set to its P_{1dB} compression point and the IM31 and IM32 components are suppressed to their lowest possible level. Then, both absorption control signals are varied equally in amplitude and phase. Figure 19 a) shows a contour plot of the measured sensitivity of the LML to such variations. A suppression of 20dB of both IM3 products requires an amplitude and phase accuracy of approximately 1.5dB and 10 , respectively. Since the LML operates at the output of the main PA, it can target specific IMD tones independently of one another without affecting the rest (as long as the control PAs operate in their linear regime). This ability to target tones independently is highlighted by the similar trajectories of the IM31 and IM32 attenuation contours, which will relax the amount of digital computation required. This is not the case for DPD even in the memory-less example, however, as shown in Fig. 19 b). The same procedure is repeated for the DPD arrangement - first the IM31 and IM31 are suppressed to their lowest possible level, then both control signals are varied.

A suppression of 20dB of both IM3 products requires an amplitude and phase accuracy of approximately 1.0dB and 5 , respectively. This is directly related to the additional higher-order tones that are indirectly generated by the DPD correction tones, which introduce interdependencies. This undesired behaviour prevents the DPD from being effective at higher compression levels. The complex interaction of the correction

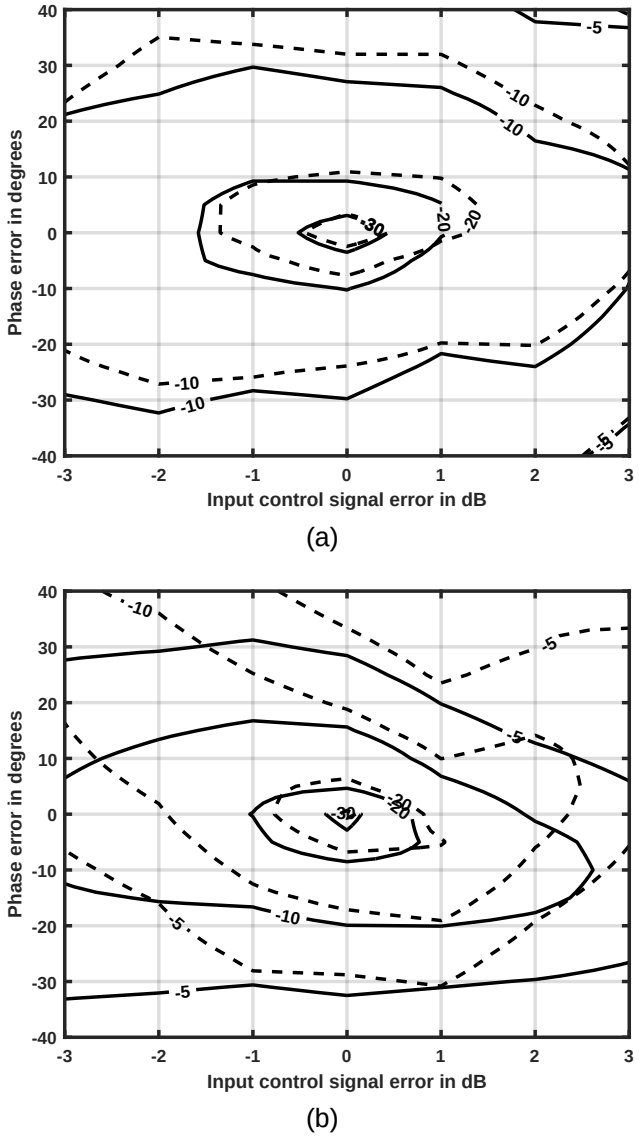

Fig. 19. Achieved IM3 suppression when the amplitude and phase of both cancellation tones are varied. Suppression of IM31 is in black and IM32 is dashed. The heatmap measurements are performed at the P_{1dB} compression point of the main PA. (a) LML and (b) DPD

tones with the IMD products is clearly visible in how different the IM31 and IM32 attenuation contours are from one another.

V. Conclusion

In this work we have presented a general framework for analyzing the active input impedances of a network with arbitrary terminations and connected to active devices. The complete network solution also provides insights into the effect of output load mismatch on the active input impedance seen by the active devices. By applying it to standard quadrature couplers, we have shown that several seemingly different systems such as diode linearizers, balanced amplifiers and the LMBA share key properties and can be classified in terms of current relations and load-modulation capabilities. In addition, a broad design categorisation based on their current boundary conditions has been presented which we hope to be insightful for others to further explore the many still hidden variations of microwave devices, whose properties can then be further developed.

We have developed the underlying theory of using active load-modulation to the problem of PA linearization in a feed-forward configuration. The design is similar in arrangement to the LMBA and achieves two key tasks - it is capable of coupling all desired power towards the output in a lossless manner, and is also able to fully absorb unwanted OOB power. The performance of the LML is not dependent on the choice of topology of the main PA, only on the amount of wanted main power and unwanted distortion power generated by it. The LML combines the power conservation properties of the LMBA with the ability to linearize at a very low power and complexity penalty. The power coupling and power absorbing mechanisms oppose each other in terms of optimal output impedance of the control PAs and require knowledge of the amplitude and phase relations of the desired tones and the unwatend IMD products at the output of the PA. The minimum available control power per device necessary to both couple and absorb a given amount of wanted and unwanted power is simply the geometric mean of the total main and total distortion powers.

The proposed mechanism is capable of easily absorbing unwanted AM/AM distortion, however it cannot correct for AM/PM distortion. This is due to the fact that the LML needs to ”lock-on” on to the signals it couples and absorbs. This makes the LML a very complimentary addition to existing DPD systems, which can easily correct for AM/PM distortion, but otherwise struggle with AM/AM distortion at high compression levels.

The LML operates at the main PA's output and it neither influences the IMD mechanisms, nor does it constrain the output power like DPD does. The system achieves IMD suppression of about 30dB, while the main PA operates at P_{3dB} and above, with a phase and amplitude error tolerance of 2 degrees and 0.5 dB, respectively. Additionally, IMD components not load-modulated by the LML are passively attenuated due to the mismatch between Z_{out} and Z_0. When the main PA is in OBO the LML achieves similar IMD suppression as DPD, making it a suitable complement to existing DPD systems.

References

[1] F. Raab, P. Asbeck, S. Cripps, P. Kenington, Z. Popovic, N. Pothecary, J. Sevic, and N. Sokal, “Power Amplifiers and Transmitters for RF and Microwave,” *IEEE Transactions on Microwave Theory and Techniques*, vol. 50, no. 3, pp. 814–826, 2002.

[2] A. Katz, J. Wood, and D. Chokola, “The Evolution of PA Linearization: From Classic Feedforward and Feedback Through Analog and Digital Predistortion,” *IEEE Microwave Magazine*, vol. 17, no. 2, pp. 32–40, 2016.

[3] F. H. Raab, “Efficiency of Doherty RF Power-Amplifier Systems,” *IEEE Transactions on Broadcasting*, vol. BC-33, no. 3, pp. 77–83, 1987.

[4] W. Wang, S. Chen, J. Cai, X. Y. Zhou, W. S. Chan, G. Wang, and Q. Xue, “A Dual-Band Outphasing Power Amplifier Based on Noncommensurate Transmission Line Concept,” *IEEE Transactions on Microwave Theory and Techniques*, vol. 68, no. 7, pp. 3079–3089, 2020.

[5] D. J. Shepphard, J. Powell, and S. C. Cripps, “An Efficient Broadband Reconfigurable Power Amplifier Using Active Load Modulation,” *IEEE Microwave and Wireless Components Letters*, vol. 26, no. 6, pp. 443–445, 2016.

[6] Y. Liu, Z. Long, M. Zhang, X. Wei, X. Xia, S. Shao, and Y. Tang, “Out-of-Band Digital Predistortion for Power Amplifiers With Strong Nonlinearity,” *IEEE Transactions on Broadcasting*, pp. 1–16, 2022.

[7] D. Pozar, "The active element pattern," *IEEE Transactions on Antennas and Propagation*, vol. 42, no. 8, pp. 1176–1178, 1994.

[8] X. Chen, S. Zhang, and Q. Li, "A review of mutual coupling in mimo systems," *IEEE Access*, vol. 6, pp. 24 706–24 719, 2018.

[9] R. T. Maximidis, D. Caratelli, G. Toso, and A. B. Smolders, "Design of Overlapped Subarrays Based on Aperture Reactive Loading," *IEEE Transactions on Antennas and Propagation*, vol. 68, no. 7, pp. 5322–5333, 2020.

[10] V. Palazzi, D. Schreurs, and R. Caverly, "The MTT-S Technical Coordinating and Future Directions Committee: Promoting Our Technical Communities-2022," *IEEE Microwave Magazine*, vol. 23, no. 11, pp. 100–141, 2022.

[11] A. N. Atanasov, W. R. A. M. Ahmad, M. S. Oude Alink, and F. E. van Vliet, "The Load-Modulated Linearizer: A Technique for Intermodulation Cancellation in PA Systems," in *2022 IEEE BiCMOS and Compound Semiconductor Integrated Circuits and Technology Symposium (BCICTS)*, 2022, pp. 174–177.

[12] P. H. Pednekar and T. W. Barton, "RF-input Load Modulated Balanced Amplifier," in *2017 IEEE MTT-S International Microwave Symposium (IMS)*, 2017, pp. 1730–1733.

[13] R. Quaglia and S. Cripps, "A Load Modulated Balanced Amplifier for Telecom Applications," *IEEE Transactions on Microwave Theory and Techniques*, vol. 66, no. 3, pp. 1328–1338, 2018.

[14] R. Quaglia, J. Pang, S. C. Cripps, and A. Zhu, "Load-Modulated Balanced Amplifier: From First Invention to Recent Development," *IEEE Microwave Magazine*, vol. 23, no. 12, pp. 60–70, 2022.

[15] Z. Qin, L. Xia, S. Lv, and B. Kong, "A W-band Diode-Based Analog Predistortion Linearizer for Traveling Wave Tube Amplifiers," in *2019 IEEE Asia-Pacific Microwave Conference (APMC)*, 2019, pp. 327–329.

[16] R. Zhou, X. Xie, B. Yan, and S. Li, "A Millimeter-Wave Predistortion Linearizer for Traveling Wave Tube Amplifiers," in *2012 International Conference on Microwave and Millimeter Wave Technology (ICMMT)*, vol. 1, 2012, pp. 1–3.

[17] H. Anton and C. Rorres, *Elementary Linear Algebra: Applications Version*, 11th ed. Wiley, 2014.

[18] R. Marks and D. Williams, "A General Waveguide Circuit Theory," 1992-10-01 1992.

[19] S. Maas, *Nonlinear Microwave and RF Circuits*, ser. Artech House microwave library. Artech House, 2003. [Online]. Available: https://books.google.nl/books?id=rY5AnwEACAAJ

[20] R. Quaglia, J. R. Powell, K. A. Chaudhry, and S. C. Cripps, "Mitigation of Load Mismatch Effects Using an Orthogonal Load Modulated Balanced Amplifier," *IEEE Transactions on Microwave Theory and Techniques*, vol. 70, no. 6, pp. 3329–3341, 2022.

[21] J. Walker, J. Custer, and M. Edwards. (2020, Oct.) Analyzing the VSWR Withstand Capability of a Balanced Amplifier. [Online]. Available: https://www.microwavejournal.com/articles/34711-analyzing-the-vswr-withstand-capability-of-a-balanced-amplifier

[22] S. C. Cripps, "Coupling Factors [Microwave Bytes]," *IEEE Microwave Magazine*, vol. 22, no. 3, pp. 12–87, 2021.

[23] J. Sun, F. Lin, H. Sun, W. Chen, and R. Negra, "Broadband Three-Stage Pseudoload Modulated Balanced Amplifier With Power Back-Off Efficiency Enhancement," *IEEE Transactions on Microwave Theory and Techniques*, vol. 70, no. 5, pp. 2710–2722, 2022.

[24] V. Qunaj and P. Reynaert, "A Ka-Band Doherty-Like LMBA for High-Speed Wireless Communication in 28-nm CMOS," *IEEE Journal of Solid-State Circuits*, vol. 56, no. 12, pp. 3694–3703, 2021.

[25] J. Pang, C. Chu, Y. Li, and A. Zhu, "Broadband RF-Input Continuous-Mode Load-Modulated Balanced Power Amplifier With Input Phase Adjustment," *IEEE Transactions on Microwave Theory and Techniques*, vol. 68, no. 10, pp. 4466–4478, 2020.

[26] Y. Cao, H. Lyu, and K. Chen, "Asymmetrical Load Modulated Balanced Amplifier With Continuum of Modulation Ratio and Dual-Octave Bandwidth," *IEEE Transactions on Microwave Theory and Techniques*, vol. 69, no. 1, pp. 682–696, 2021.

[27] A. A. Muller, P. Soto, D. Dascalu, D. Neculoiu, and V. E. Boria, "A 3-D Smith Chart Based on the Riemann Sphere for Active and Passive Microwave Circuits," *IEEE Microwave and Wireless Components Letters*, vol. 21, no. 6, pp. 286–288, 2011.

[28] B. Kim, "Chapter 2 - Power Amplifier Fundamentals," in *RF and mm-Wave Power Generation in Silicon*, H. Wang and K. Sengupta, Eds. Oxford: Academic Press, 2016, pp. 17–58.